Available online at www.sciencedirect.com

SciVerse ScienceDirect

Energy Procedia 22 (2012) 127 – 136

Energy Procedia

Symposium T: Materials for solar hydrogen via photoelectrochemical production

Efficient Anodically Grown WO_3 for Photoelectrochemical Water Splitting

S. Caramori[(a)]*, V. Cristino[(a)], L.Meda[(b)], A. Tacca[(b)], R. Argazzi[(c)] and C.A. Bignozzi[(a)]*

(a) Dipartimento di Chimica dell'Università di Ferrara, Via Luigi Borsari 46, 44121 Ferrara, Italy

(b) Istituto ENI Donegani , Via Fauser 4, 28100, Novara, Italy

(c) ISOF CNR c/o Dipartimento di Chimica dell'Università di Ferrara, Via Luigi Borsari 46, 44121 Ferrara, Italy

Abstract: The potentiostatic anodization of metallic tungsten has been investigated in different solvent/electrolyte compositions with the aim of improving the photoelectrochemical performances of the tungsten oxide layer. Among the explored electrolytes, the anodization in the NMF/H_2O/NH_4F solvent mixture was found to produce the most efficient WO_3 photoanodes, which, combining spectral sensitivity, high electrochemically active surface and improved charge transfer kinetics, outperform, under simulated solar illumination, most of the reported nanocrystalline substrates produced by anodization in aqueous electrolytes and by sol gel methods. While the preparation of the photoelectrodes is a slow process at room temperature (20 °C), it could be greatly accelerated (x 10) by carrying out the anodization at 40-50 °C, thus proving to be a fast and convenient approach to the production of high performing WO3 photoactive substrates directly connected to a metal electron collector .

Keywords: WO_3; anodization; nanostrcutres, photoelectrochemistry

1876-6102 © 2012 Published by Elsevier Ltd. Selection and/or peer review under responsibility of European Material Research Society (E-MRS)
Open access under CC BY-NC-ND license. doi:10.1016/j.egypro.2012.05.214

1. 1. Introduction

Since the experiment of Fujishima and Honda[1], the use of semiconductor photoelectrodes or nanoparticles, have appeared to be an interesting and viable approach to the photoinduced water splitting (i.e. the splitting of the water molecule in molecular oxygen and hydrogen), thanks to the possibility to convert, with high quantum yield, UV-vis radiation in highly energetic charge carriers that can induce the required electrochemical reactions at the solid/electrolyte interface[2-5].

Photoanodes based on n-type metal oxides like TiO_2[6], WO_3[7] and Fe_2O_3[8,9] have been intensely studied, since, they couple ease of fabrication, high chemical stability in aqueous solution under evolving oxygen conditions, and reasonably high efficiency when operated in a photoelectrochemical cell. Particularly, WO_3 electrodes show interesting properties displaying both visible absorption and good charge transport abilities[10-12]. Tungsten (together with Al, Ti, Zr, Bi, Ta, Nb) belongs to the group of the so called valve metals, which passivate and show a very high corrosion resistance in most common aqueous media. The composition of naturally or anodically formed tungsten oxide films is essentially coincident with that of WO_3[13]. Thus, electrochemical anodization of metallic tungsten can be a convenient method for preparing porous photoactive films in which the oxide structures are tightly interconnected and strongly bound to the metal collector, both factors concurring to increase the photogenerated charge collection efficiency. It has already been shown that by this approach it is indeed possible to obtain interesting nanostructures that can find application in the field of solar energy conversion[14,15].

The most common route for the anodic preparation of porous WO_3 films involves the application of a constant potential to a metallic tungsten lamina in the presence of aqueous electrolytes containing fluoride anions which establish mild oxide dissolution conditions. It is the achievement of a steady state between oxide dissolution and formation which leads to nanotubular or nanoporous structures. Some authors have also achieved a porous oxide structure (and even some small nanotubular WO_3 domains) by careful application of an appropriate overvoltage intended to reach oxide breakdown conditions in fluoride free electrolytes[16]. Basically, in order to reach breakdown conditions, made possible by the presence of a strong applied field, a harsh treatment consisting in the application of a sudden potential step of several tens of volts has to be adopted. Electrolyte temperature and compositions are also important for reaching reproducible results and a reasonable surface coverage. Although in some contributions it appears that the monochromatic conversion in the visible region has been optimized following certain annealing conditions (pure oxygen atmosphere, 550 °C)[10], more often are found literature reports in which the nanostructured WO_3 substrates display an high photoactvity in the UV region but give a limited response in the visible frequencies. This is consistent with the reported monoclinic WO_3 indirect band gaps apparently ranging from 3.25 to 2.9 eV[15,17]. Indeed, we have also verified that, by following or slightly modifying literature approaches, relevant IPCEs in the order of 50 % or higher could be reached in the UV region, but no substantial photoactivity could be observed beyond 430 nm. We started therefore a systematic investigation on the effect of the electrolyte composition on the photoelectrochemical properties of anodized WO_3 electrodes. Our work has been largely inspired by the studies of Grimes et al.[18] on the anodic formation of titania nanotubes. We report here on the preparation and characterization of WO_3 electrodes which combine a large spectral sensitivity to improved charge transfer kinetics and allow for high production yields of hydrogen in 1M H_2SO_4 under a potential bias of 1V vs SCE.

2. Experimental Section

2.1. Materials

Metallic tungsten foils 99.95% (0.1 mm thick), N-methyl-formamide (NMF), formamide, dimethyl sulfoxide (DMSO), N,N- dimethyl-formamide (DMF), hydrofluoric acid were from Alfa Aesar. Ammonium fluoride,

Alconox, sulphuric acid, ethanol, methanol, acetone, were reagent grade products obtained from Fluka or Sigma-Aldrich and used as received. Nanocrystalline WO_3 electrodes obtained by blading of a sol-gel precursor on fluorine-tin oxide conductive glass substrates (FTO, TEC 8, 8 ohm/□, from Hartford Glass, USA) were prepared according to literature procedures [19,20].

2.2. Preparation of WO3 photoanodes

Prior to anodization, tungsten foils ca. 2 x 1 cm were sonicated in an aqueous alconox solution for 10 minutes, rinsed with water and washed with ethanol and acetone. The potentiostatic anodization was carried out in a two electrode configuration in which the tungsten anode and cathode were cofacially assembled at an average distance of 3 mm. By using a DC power supply (KERT Cosmo 1500/1), the voltage was quickly manually increased to the final value of 40 V, with a rate of approximately 0.5 V/s. The best electrolyte was composed by NMF/H_2O 8/2 and 0.05 % NH_4F w/w. An increase in fluoride concentration up to 0.1 % led to identical results. The use of an equivalent (with respect to NH_4F) molar amount of HF instead of NH_4F did not change the structure and the performance of the resulting oxide surface. Electrolytes based on other high dielectric constant organic solvents (DMSO, formamide, DMF, ethylene glycol) were explored in an analogous ratio, i.e. organic solvent/water 8:2 in the presence of ammonium fluoride or HF (0.05 – 0.1 % w/w) with less satisfactory results. The solution was kept unstirred and the anodization was carried out for 72 hours at room temperature (20±3 °C). The typical average current density during the anodization in NMF was 4-6 mA/cm^2 and the total charge exchanged, obtained by integration of the i-t curve was 150±18 C. The accelerated anodization processes at higher temperatures was carried out in a thermostatic bath. Temperatures of both 40 °C and 50 °C were explored. Under these conditions the anodic current reached maximum values close to 55 mA/cm^2.

After the anodization process, the resulting WO_3 electrodes were rinsed with water, ethanol and acetone and sonicated in water for 10 minutes in order to remove weakly surface bound material or debris, dried under an air stream and fired at 550 °C in air for 1 hour to promote sintering and crystallization.

2.3. Photoelectrochemical Measurements

J-V curves were recorded with an Eco Chemie PGSTAT 302/N potentiostat in a three electrode configuration by using a Pt wire counter electrode and a SCE reference electrode. The typical scan rate was 20 mV/s. Simulated sunlight irradiation was obtained with an ABET sun simulator equipped with a 150 W Xe lamp and an AM1.5 G filter. Incident irradiance was measured with a Molectron Power Max 500 power meter.

IPCE spectra (n° of collected electrons/n° of incident photons) were obtained by using the same three electrode cell described above, by using a 150 W water cooled Xe lamp coupled to an Applied Photophysics monochromator (1200 lines/mm, f:4, band pass 10 nm). The photocurrents were recorded with an Agilent 34401A 6 ½ digits multimeter. The potential bias was generated by an AMEL mod. 552 potentiostat. Incident irradiance was measured by a Centronic OSD 7Q calibrated photodiode

Potentiostatic electrochemical impedance spectroscopy (EIS) was performed by using an Eco Chemie Frequency response analyzer by applying a single sinusoidal perturbation of the amplitude of 10 mV in the 5 10^4 – 5 10^{-3} Hz frequency range. The response was acquired with the Eco Chemie Nova 1.5 program and fitted in terms of equivalent circuits with Z-Simp Win 3.22 software. In all cases the experimental data could be satisfactorily fitted in terms of simple equivalent circuits of the type R(QR') where R is the ohmic resistance, R' is the interfacial charge transfer resistance and Q is the constant phase element accounting for the non ideal double layer capacitance.

3. Results and Discussion

3.1. Formation of Anodically grown WO_3

A NMF based electrolyte was privileged because of the high dielectric constant of such solvent (182.4), which may favor, at any given potential, the formation of a higher charge density on the oxide layer, improving the extraction of W^{6+} and, ultimately favoring oxide growth. In this electrolytic composition water is required to act as an oxygen donor allowing for oxide formation., while fluorides act as a chemical etchant, promoting localized oxide dissolution and the formation of corrosion pits from which the field assisted dissolution is stronger. After 72 h at room temperature, the anodization in NMF results, after subsequent annealing, in the formation of an irregular porous nanocrystalline (monoclinic) oxide layer 3-5 micron thick, with bundled up structures, ca. 300 nm wide, longitudinally crossed by cracks which give to the surface an overall worm-like appearance (Fig.1). The AFM imaging gives the topographical picture of the surface, confirming the existence of such morphology and revealing a maximum height difference between structure crests and valleys or pores of approximately 600 nm.

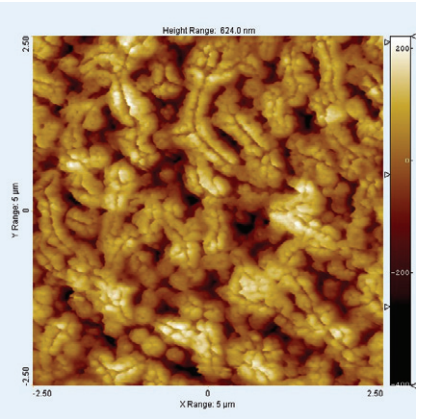

Fig.1 AFM micrograph of anodically formed WO_3 after the annealing process at 550 C° for 1 h in air

The SEM imaging of WO_3 films obtained at progressive anodization time intervals in the NMF electrolyte provides a picture of the stages involved in the formation of the photoactive oxide. After 2 hours from the beginning of the anodization a compact oxide layer with few corrosion pits is evident (Fig.2). After 6 hours the number of pits is increased and thicker oxide walls are present at their borders, suggesting oxide growth and formation of deeper tubes with a circular mouth. With the progress of the anodization, the adjacent tubes grow in number, their walls grow in thickness, coalesce and crack, finally resulting, after 24 h, in the characteristic surface which is still observed after 48 and 72 hours. The same surface morphology is observed also in WO_3 samples obtained through the accelerated anodization route at 40 °C, in which nano tubular domains can also be noted (Fig. 3 (A), (B)). This analogy suggests that also under these conditions the formation of the oxide follows essentially the same stages which are observed at room temperature. Simply, the kinetics of both the competing processes, i.e. oxide formation and dissolution, are improved, as demonstrated by the significantly higher currents (40-50 mA/cm^2 recorded at 40 °C compared to 4-6 mA/cm^2 at R.T.) observed during the accelerated anodization process (Fig.3C). After an initial interval (ca. 30 min) during which the current is very low, due to the presence of a compact oxide barrier layer, a steep rise of the anodic current follows, indicating that both chemical etching by F^- ions and field assisted oxide dissolution coupled to the concomitant formation of fresh WO_3 from the underlying metal are now taking place. The competition between these two processes determines the inward movement of the W/WO_3 interface and the formation of an outer porous oxide film which can reach a thickness of few microns (Fig.3C).

The fact that the current continues to maintain relevant values (> 25 mA/cm^2) along the whole duration of the anodization process and the observation of gas bubbles evolving from the oxide surface under anodization indicate the persistence of ionic and electronic conduction through the W/WO_3 interface.

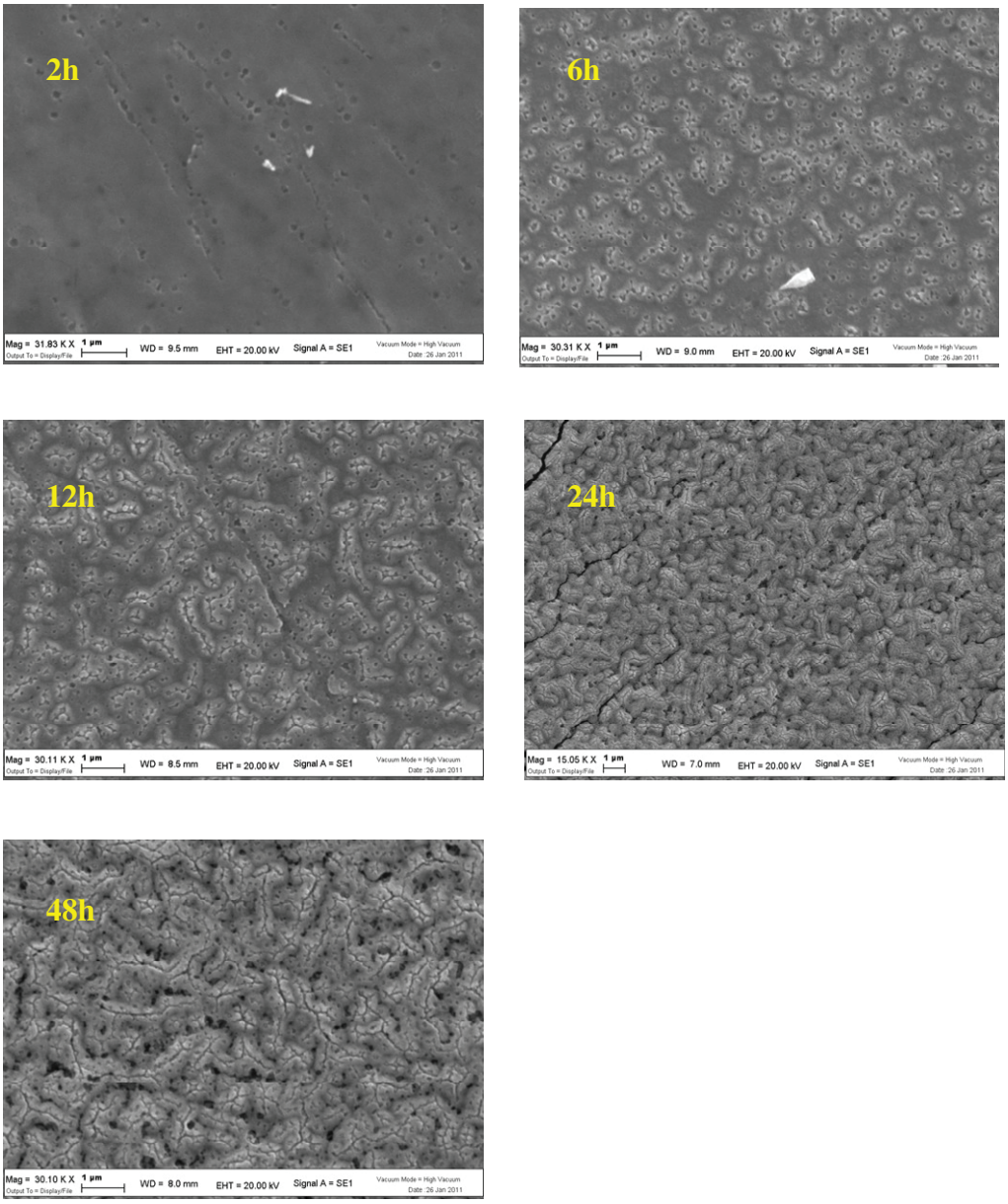

Fig.2 - SEM micrographs of the WO_3 surface resulting from the anodization in the NMF based electrolyte at different times: 2 h, 6 h, 12 h, 24 h, 48 h. Samples annealed at 550 °C in air before SEM imaging.

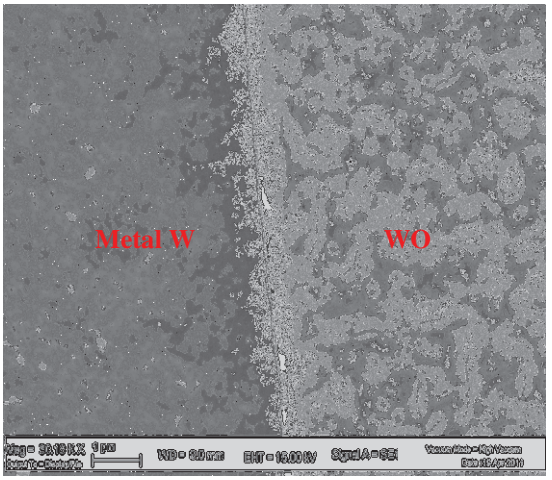

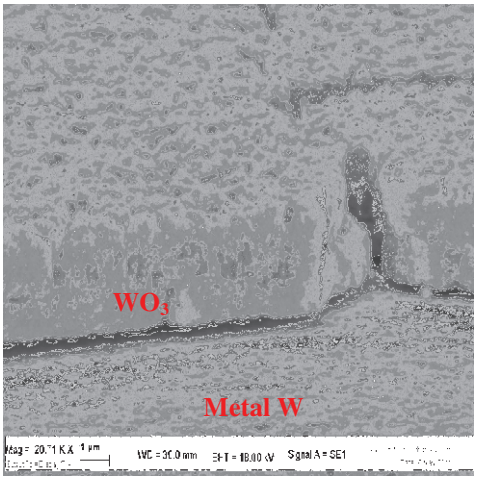

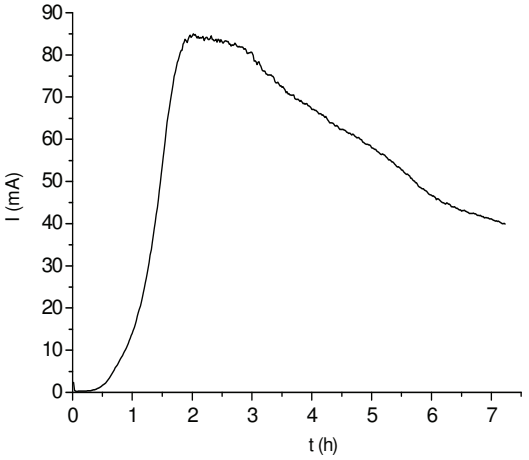

Fig.3. SEM top (A) and cross sectional (B) micrographs of the WO_3 film after 7 hours of the accelerated anodization in the NMF based electrolyte at 40 °C. Samples annealed at 550 °C in air before SEM imaging. (C) typical current-time (i-t) behavior recorded during anodization.

3.2. Photoelectrochemistry

When compared to colloidal WO_3 films[20] obtained by blade casting or to other samples obtained by anodization in different solvents (DMF, DMSO, water), the typical photoelectrochemical performances of the WO_3 films grown in NMF are relevant: under an incident power of 0.15 W/cm^2 (AM 1.5 G) these samples deliver the highest photocurrent, approaching 3.5 mA/cm^2 at 1.5 V vs SCE. Interestingly, a double layer colloidal electrode obtained by two subsequent blade casting, with a thickness comparable to the NMF substrate, undergoes only a marginal improvement over the single layer, suggesting that the oxide thickness or the related light harvesting

alone is not entirely responsible for the different performances. Other factors, presumably charge transport and charge transfer resistance at the interface and specific electro active surface area are playing the major role in determining the photoelectrode behavior.

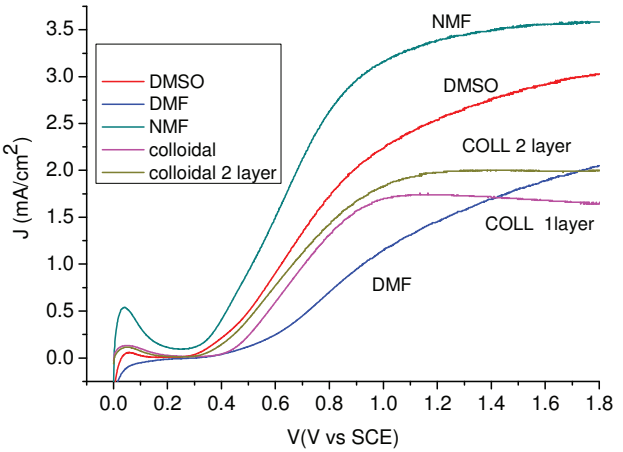

Fig.4. J-V curves in 1M H_2SO_4 for anodized WO_3 films obtained from different electrolytic compositions : NMF (dark cyan), DMF (blue), DMSO (red), colloidal (gold and purple) . AM 1.5 G, 0.15 W/cm^2

Under AM 1.5 G incident irradiation, the photocurrent generated by photoelectrodes obtained from the NMF route, varies in a reasonably linear fashion with the incident irradiance, showing maximum values exceeding 9 mA/cm^2 under 0.37 W/cm^2 with an average slope of 0.013 A cm^{-2} V^{-1}. The advantage of the electrochemically grown WO_3 over a more conventional WO_3 electrode obtained by standard sol-gel methods (colloidal), can be clearly appreciated from Fig.5: while the performances of the two electrodes are quite similar at low power intensities, under strong illumination the anodically grown film does not show saturation and clearly outperforms the colloidal film by almost a factor of four, indicating, particularly under high power intensities, a more effective hole transfer to the electrolyte.

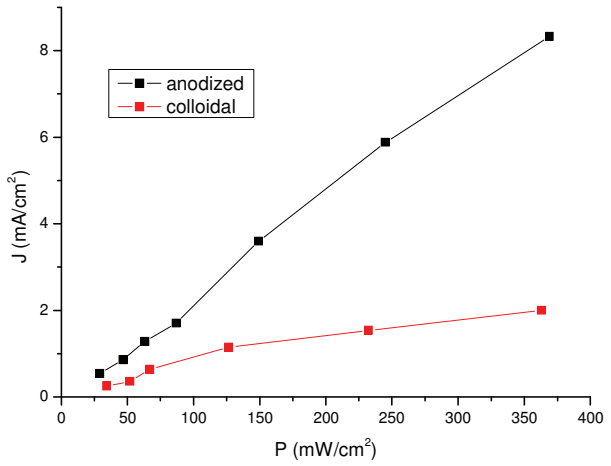

Fig.5. Photocurrent density taken at 1 V vs SCE as a function of the incident irradiance (AM 1.5 G): (black) anodically grown; (red) sol/gel WO_3

In the presence of an electrolyte composed by 1 M H_2SO_4/CH_3OH 8/2 (V/V) the plateau photocurrents generated by the anodically grown WO_3 films are nearly doubled, approaching, under strong illumination (ca. 0.3 W/cm^2), 16 mA/cm^2. Concomitantly, it can be observed a negative shift of the photoanodic onset of ca. 100 mV: both effects are consistent with an improved hole scavenging by CH_3OH and/or by a known mechanism of photocurrent doubling from surface adsorbed highly reducing $CH_3O\cdot$ intermediates[21]. A further evidence of effective charge transfer to the electrolyte, as well as of photocurrent doubling in the presence of methanol, acting as a hole scavenger, was gained from the J-V curves recorded under shuttered illumination, in which the rectangular shape of the transients, the presence of small photoanodic transients in the immediate proximity of the flat band potential and the lack of cathodic features are all indicative of efficient photoinduced charge separation and transport[22].

As indicated by a recently published study[23], the good photoelectrochemical properties of the anodically grown WO_3 in NMF stem from a low charge transfer resistance and from a highly porous surface formed by interconnected nanostructures which enhance the possibility of hole transfer to the electrolyte and the concomitant electron transport to the metal collector.

These properties are retained in samples obtained from the accelerated (40 °C) anodization route, as demonstrated by the IPCE spectra (Fig.6(A)) recorded in sulfuric acid, which, in the best case (10 h anodization), approach 75 % in a broad region in the UV, extending deeply in the visible region thanks to a secondary maximum at 390 nm ($IPCE_{max}$ = 65-70 % at 1.5 V vs SCE). The photoaction onset is located at 480 nm. As a comparison, WO_3 films electrochemically produced either in water/HF/NH_4F according to the procedure described by Guo et.al,[15] or in other organic solvents like DMF or by sol gel methods, do not show any relevant photoconversion beyond 430-440 nm. This indicates that, thanks to the high porosity of WO_3 films produced by anodization in NMF, the hole transfer to the electolyte has been optimized, allowing to achieve charge separation and conversion also at those wavelengths close to the visible absorption threshold of the oxide (430-470 nm). Indeed, visible photons with a longer penetration depth in the material, often create electron hole pairs in the inner part of the oxide where, due to a poor permeation by the electrolyte, losses by recombination are more likely to occur. Both in terms of IPCE and of J-V characteristics, the performances of the photoelectrodes obtained at 40 °C in the anodization interval comprised between 10 and 7 hours are, within the experimental error, essentially comparable (Fig.6 (B)), proving that the accelerated anodization route is a rather reproducible procedure which does not depend critically, at least within a reasonably wide time interval, from the duration of the anodization process.

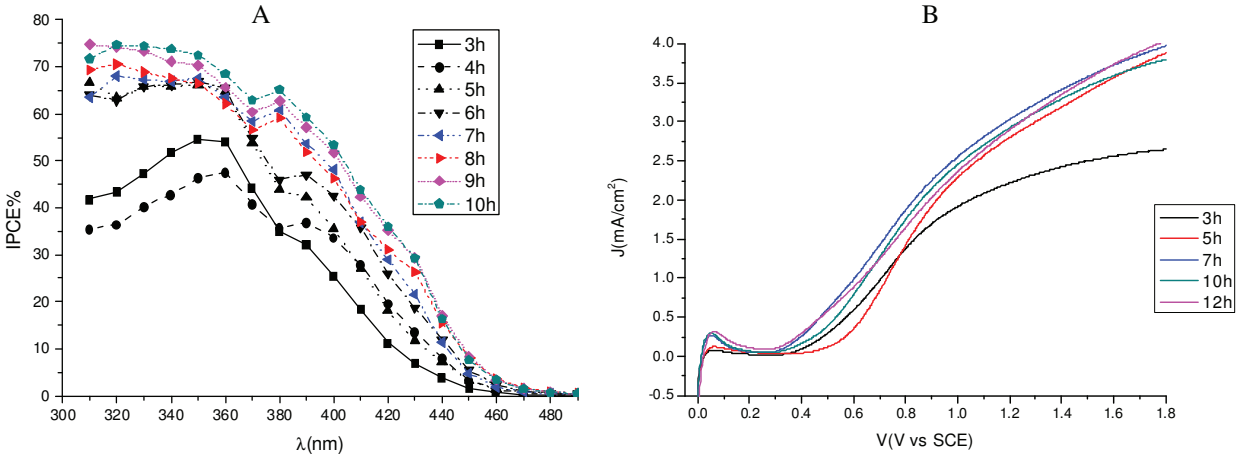

Fig.6. (A) IPCE spectra of anodically grown WO_3 samples obtained in accelerated anodization conditions (3-10 h) biased at 1.5 v vs SCE. 1 M H_2SO_4 (B) J-V curves of anodically grown WO_3 obtained in accelerated anodization conditions (3-12 h) 1 M H_2SO_4, 0.2 W/cm^2.

At 50 °C the electrochemical growth of the oxide is faster and the anodization process can be controlled with less accuracy, showing, for example, a large difference in the photoelectrochemical response of samples obtained in

a relatively narrow time interval (e.g. 1-2 h). Nevertheless the results are encouraging, since a good IPCE (70 %) and a reasonable extension to the visible region up to 470 nm can be obtained just after 2 hours of anodization. However the performances of the electrodes rapidly decay by increasing the anodization time probably due to an excessive thickness of the resulting WO_3 layer in which the transport and the interfacial transfer of the charge carriers become more critical, as suggested by the modest average slope (2mA/V) of the J-V characteristics. In some cases (*but not always)* the poorer performance is also associated to the loss of the typical worm-like structure, which is replaced by sintered nano particles or by a not well resolved, even at the highest SEM magnification allowed by our machine (10^5 X), needle network. Such changes in surface and film morphology may also introduce modifications in the carrier transport across the film, leading to a less effective charge separation and collection. This is indicated also by the Nyquist plots recorded at 0.7 V vs SCE under 0.2 W/cm^2 AM1.5 G illumination, which reveal a larger charge transfer resistance (Rct ~ 200 ohm in the most favorable case) in the samples anodized at 50 °C with respect to the typical samples obtained at 40 °C (Rct ~150 Ohm) (Fig.7).

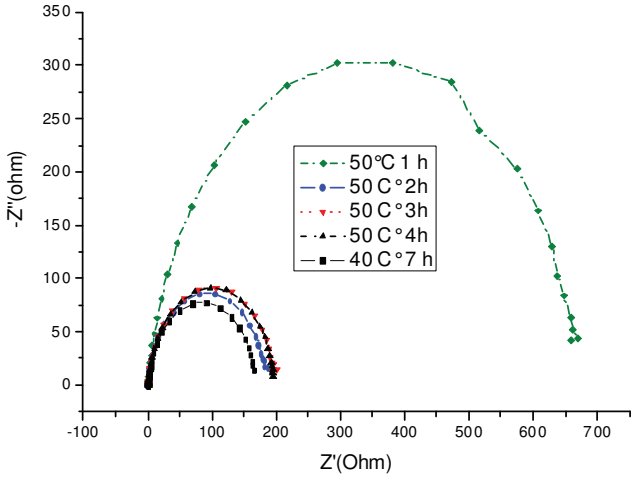

Fig. 7. Nyquist plots recorded at 0.7 V vs SCE under 0.2 W/cm^2 Am 1.5 illumination for anodized samples obtained under accelerated conditions at 50 °C (1-4 h) compared to a typical WO_3 sample obtained at 40 °C (7h)

4. Conclusions

The anodization of tungsten in the NMF/H_2O/NH_4F electrolyte leads to the formation of highly efficient WO_3 films, which, combining spectral sensitivity, high electrochemically active surface and low interfacial charge transfer resistance can find a promising application as photoanodes in photoelectrolytic cells for solar water splitting. The preparation of the photoelectrodes can be significantly accelerated at the temperature of 40 °C without negative repercussions on the photoelectrochemical performance, proving to be a fast and convenient approach to the production of high performing WO_3 photoactive films directly connected to a metal electron collector .

Aknowledgements

Funding from ENI is gratefully acknowledged.

References

[1] Fujishima, A.; Honda, K. *Nature* 1972, *238*, 37.
[2] Pleskov, Y. Y.; Guerevich, Y. Y. *Semiconductor Photoelectrochemistry*; Plenum Publishing Co.: New York, 1986.
[3] Tan, M. X.; Laibnis, P. M.; Nguyen, S. T.; Kesselman, J. M.; Stanton, C. E.; Lewis, N. S. *Progress in Inorganic Chemistry*; John Wiley & Sons: New York, 1994, 21-144.
[4] Hagfeldt, A.; Graetzel, M. *Chem.Rev.* 1995, *95*, 49-68.
[5] Nozik, A. J.; Memming, R. *J.Phys.Chem.* 1996, *100*, 13061-13078.
[6] Chen, X.; Mao, S. S. *Chem.Rev.* 2007, *107*, 2891-2959.
[7] Wang, H.; Lindgren, T.; He, J.; Hagfeldt, A.; Lindquist, S.-E. *J.Phys.Chem.B.* 2000, *104*, 5686-5696.
[8] Khan, S. U. M.; Akikusa, J. *J.Phys.Chem.B.* 1999, *103*, 7184-7189.
[9] Sartoretti, C. J.; Alexander, B. D.; Solarska, R.; Rutkowska, I. A.; Augustynski, J.; Cerny, R. *J.Phys.Chem.B.* 2005, *109*, 13685-13692.
[10] Santato, C.; Odziemkowski, M.; Ulmann, M.; Augustynski, J. *J.Am.Chem.Soc.* 2001, *123*, 10639-10649.
[11] Santato, C.; Ulmann, M.; Augustynski, J. *J.Phys.Chem.B.* 2001, *105*, 936-940.
[12] Bard, A. J.; Park, J. H. *Electrochemical and Solid State Letters* 2006, *9*, E5-E8.
[13] Metikos-Hukovic, M.; Grubac, Z. *Journal of Electronanalytical Chemistry* 2003, *556*, 167-178.
[14] Tsuchiya, H.; Macack, J. M.; Sieber, I.; Taveira, L.; Ghicov, A.; Sirotna, K.; Schmucki, P. *Electrochem. Commun.* 2005, *7*, 295-298.
[15] Guo, Y.; Quan, X.; Huimin Zao, N. L.; Chen, S. *Environ.Sci.Technol.* 2007, *41*, 4422-4427.
[16] Hahn, R.; Macak, J. M.; Schmuki, P. *Electrochemistry Communications* 2007, *9*, 947-952.
[17] Berger, S.; Tsuchiya, H.; Ghicov, A.; Schmucki, P. *Appl. Phys. Lett.* 2006, *88*, 203119-203121.
[18] Paulose, M.; Shankar, K.; Yoriya, S.; Prakasam, E. H.; Varghese, O. K.; Mor, G. K.; Latempa, T. A.; Fitzgerald, A.; Grimes, C. A. *J.Phys.Chem.B. Letters* 2006, *110*, 16179-16184.
[19] Angiuli, F.; Argazzi, R.; Caramori, S.; Bignozzi, C. A. *Patent WO 2007/094019 A1*.
[20] Meda, L.; Tozzola, G.; Tacca, A.; Marra, G. L.; Caramori, S.; Cristino, V.; Bignozzi, C. A. *Solar energy Materials & Solar Cells* 2010, *94*, 788-796.
[21] Morrison, S. R.; Freund, T. *J.Chem.Phys.* 1967, *47*, 1543-1551.
[22] Sivula, K.; Zboril, R.; Le Formal, F.; Robert, R.; Weidenkaff, A.; Tucek, J.; Frydrych, J.; Graetzel, M. *J.Am.Chem.Soc.* 2010, *132*, 7436-7444.
[23] Cristino, V.; Caramori, S.; Argazzi, R.; Meda, L.; Marra, G. L.; Bignozzi, C. A. *Langmuir* 2011, *27*, 7276-7284.